

Article

Research Regarding the Development of the Combustion Chamber of Internal Combustion Engines with Opposite Pistons

Horia Beles ^{1,†}, Adrian Tusinean ^{2,†}, Tudor Mitran ^{1,*,†}  and Florin Bogdan Scurt ^{1,†}

¹ Department of Mechanical Engineering and Automotive, University of Oradea, Universitatii St. 1, 410087 Oradea, Romania

² ThermoLift Inc., 27275 Haggerty Rd., Suite 420 Novi, Detroit, MI 48377, USA

* Correspondence: tudor_mitran@uoradea.ro; Tel.: +40-744-152-212

† These authors contributed equally to this work.

Abstract: The reduction in environment pollutant emissions is one of the main challenges regarding ground transportation. Internal combustion engines, used especially in hybrid propulsion systems, may be a solution in the transition to fully electric cars. Therefore, more efficient engines in terms of fuel consumption, emission generation and power density must be developed. This paper presents research regarding the architecture of the combustion chamber of an internal combustion engine with opposed pistons. The aim of this research was to find a combustion chamber architecture that would enable the engine to perform close to the program target of: NO_x < 3.5 g/kWh, smoke (FSN) < 1, specific fuel consumption (bsfc) < 198 g/kWh. Three variants of the combustion chamber's architecture have been studied. After the experimental research, the conclusion was that none of them fully reached the target; however, significant improvements have been achieved compared with the starting point. As a result, further research needs to be carried out in order to reach and even exceed the target.

Keywords: diesel engine; opposite pistons; combustion chamber design; pollutant emissions reduction; specific fuel consumption; energetic and ecological performances



Citation: Beles, H.; Tusinean, A.; Mitran, T.; Scurt, F.B. Research Regarding the Development of the Combustion Chamber of Internal Combustion Engines with Opposite Pistons. *Machines* **2023**, *11*, 309. <https://doi.org/10.3390/machines11020309>

Academic Editor: Chenglong Tang

Received: 23 December 2022

Revised: 15 February 2023

Accepted: 17 February 2023

Published: 20 February 2023



Copyright: © 2023 by the authors. Licensee MDPI, Basel, Switzerland. This article is an open access article distributed under the terms and conditions of the Creative Commons Attribution (CC BY) license (<https://creativecommons.org/licenses/by/4.0/>).

1. Introduction

Ground transportation is one of the major polluting sources of the environment [1–3]. The regulations adopted by the European Union (EU) countries, which have also been applied in Iceland, Liechtenstein, Norway, Switzerland, and Turkey, led to an important reduction in ground transportation air pollutant emissions. As a result, between 1990 and 2017, the emissions of nitrogen oxides decreased by 66%, the emissions of carbon monoxide and those of the non-methane volatile organic compounds decreased by 87%, and the emissions of particulate matter with a diameter of 2.5 µm, or less, decreased by 44% [4]. In Europe, different legal mechanisms impose limits on the total emissions, which also regulate the transportation sector by setting emissions standards. A proposal to reduce pollution from the new vehicles equipped with internal combustion engines sold in EU is to reach the European Green Deal's zero-pollution target [3]. To reach these objectives, it is necessary to develop new technologies. The current trend is to use hybrid electric vehicles (HEV), or full electric vehicles (EV). However, to continue this trend, it is necessary to make progress regarding the autonomy, costs, and the infrastructure for EV. For example, the current number of public charging stations in the EU is around 250,000. The predicted number of charging stations required in 2024 will be at least 1,000,000. In 2030, the predicted required number of charging stations in the EU is more than 3,000,000. By now, progress has been made for more sustainable road mobility. This can be reached by technical innovations and by governmental infrastructure investments. In Europe, the legal air limits for particulates

are met almost everywhere [5]. Various research directions have been developed to reduce polluting emissions produced by ground transportation. The most important development that should totally reduce the local pollutant emissions is the electrification of the vehicles' propulsion system. As mentioned above, there are some problems that should be solved before this solution can be used on a large scale. Another direction to reduce pollutant emissions produced by ground transportation is the development of hydrogen-based propulsion systems [6–8]. Research has been developed to replace the conventional liquid fuels (Diesel fuel in this case) with alternative ones [9,10]. The synthetic liquid fuels can also replace the conventional fuels. Therefore, another research direction is the production of such fuels [11,12]. These solutions should be used in addition to the battery electric propulsion systems. An intermediate solution can be constituted by the development of hybrid electric vehicles [13–16], especially as a part of a hybrid propulsion system where these can function in a single regime, corresponding to the minimum polluting emissions. Internal combustion engines can still be a major factor in the reduction in the pollutant emissions from ground transportation. There are still means that can be applied to reduce pollutant emissions produced by the internal combustion engines; therefore, research is still being carried out to improve Diesel engines' performances [17–20]. The aim of the research presented in this paper was to improve the energetic and ecological performances of the internal combustion engine (ICE) with opposed pistons. To reach this goal, the research was conducted in order to find a combustion chamber architecture that would enable the engine to perform close to the program target of: $\text{NO}_x < 3.5 \text{ g/kWh}$, smoke (FSN) < 1 , specific fuel consumption (bsfc) $< 198 \text{ g/kWh}$. The engine with opposite pistons and opposite cylinders (OPOC), named EM100D, subject to the research of this paper is a combination of the opposed pistons engine Jumo 205 (designed and realized by Hugo Junkers) and the Boxer engine. This EMD100D engine was chosen for the research because it takes the advantages of the two types of engines: high specific power, compactness, low specific weight, and the ability to reach high rotational speeds. Furthermore, the piston's stroke is divided in two. As a result, at the same engine's rotational speed, the mean piston's speed is significantly reduced. This leads to a reduction in the internal frictions. If the preservation of the piston's mean speed is desired, the rotational speed can be doubled. This means a doubling of the engine's power. Another advantage is the reduction in the number of cylinders and the raising of the piston displacement for one cylinder. The disadvantages of the Jumo 205 (the synchronizing of the two crankshafts through two gear wheels heavily mechanically stressed and a rigid construction of the engine block) and those of the Boxer engine (a strong stress on the cylinder block and on the crankshaft) have been removed in the EM100D engine. The EM100D has only one crankshaft, and the cylinder block is not overstressed. The disadvantages of the EM100D are those of a two-stroke engine: the difficulty to control the gas exchange process and the polluting emissions. One of the key factors that leads to a reduction in the specific fuel consumption and the pollutant emissions of an ICE engine is the way in which the combustion occurs. This research was focused on the optimization of the combustion chamber's geometry. The shape of the bowl manufactured in the piston's head has a great influence on the combustion process, so it is important to study the geometry of the combustion chamber [21,22] (pp. 310–311). Three variants of the combustion chamber's design were studied to reach a reduction in the fuel specific consumption and in the pollutant emissions (nitrogen oxides and smoke). To do so, it was necessary to design a combustion chamber to start with. After the design and the manufacture of this combustion chamber, tests were carried out to determine the engine's energetic and ecological performances. The results were not totally satisfactory, so further research was carried out to improve the engine's performances by modifying the combustion chamber's shape. This necessitated the development of an optical combustion chamber to determine the main parameters of the fuel injection and fuel spray formation and evolution. As a result of this investigation, those parameters were identified and were used for the implementation of a real combustion chamber that should improve the engine's performances. The conclusion was that, although progress has been made, the

research must continue, especially regarding the use of gaseous fuels, such as methane and hydrogen. An internal combustion engine (ICE) with low fuel specific consumption and low pollutant emissions at medium loads can be a solution for the HEV, until the problems of the EV are solved.

2. Materials and Methods

The research presented in this paper was realized on an opposed pistons opposed cylinders (OPOC) two-stroke Diesel engine and also on experimental transparent combustion chambers. The engine was built by EcoMotors International based on Prof. Hofbauer's patent [23]. This engine is a combination of the Jumo 205 engine and the Boxer engine. The concept presented in this paper eliminates some of the disadvantages of the two engines mentioned above, while implementing some of the advantages that two engines inherited. As shown in Figure 1, the OPOC engine has two opposed cylinders (as a Boxer engine), and in each of the cylinders, there are two opposed pistons (as in Jumo engine), one of the pistons governing the intake ports (intake piston) and the other governing the exhaust ports (exhaust piston). In order to increase the volumetric specific power, a two-stroke engine configuration has been chosen. The name of the engine used for this research is EM100D. The schematic of the engine with opposed pistons and opposed cylinders EM100D is presented in Figure 1.

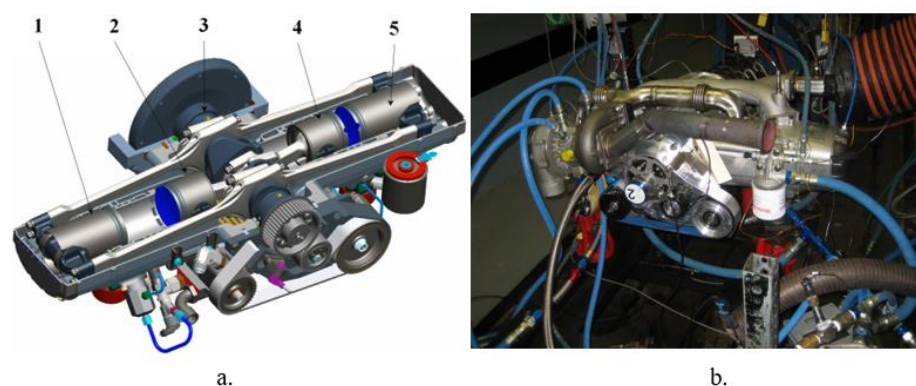


Figure 1. (a) The scheme of the engine with opposed pistons (EM100D): 1—Outer exhaust piston; 2—Inner intake piston; 3—Crankshaft; 4—Inner exhaust piston; 5—Outer exhaust piston; (b) The EM100D on the test bench.

The combustion chamber is formed between two pistons heads and is one of the fundamental elements that influences the formation and combustion of the air–fuel mixture. In a two-stroke direct injection Diesel engine, the development of the combustion chamber's geometry must be correlated with the scavenging process in the cylinders and also with the characteristics of the fuel's pulverization process (injection profile, start of the injection, fuel jet's characteristics). To establish the optimal shape of the EM100D engine's combustion chamber, an iterative analysis of the diverse possible geometries was required, the final criterion for the appreciation of a combustion chamber's qualities being the one linked to the ecological performances (NO_x , smoke) and the energetic ones (specific fuel consumption, power and torque).

The EM100D engine was installed and tested in a testing cell equipped with an Eaton AC electric brake, with a braking power of 300 kW and a limit rotational speed of 8000 rpm. The torque was measured with a contactless transducer of Eaton Lebow type with a capacity of 1000 Nm. In Figure 2, the scheme of the test bench and the scheme of the torque transducer are presented.

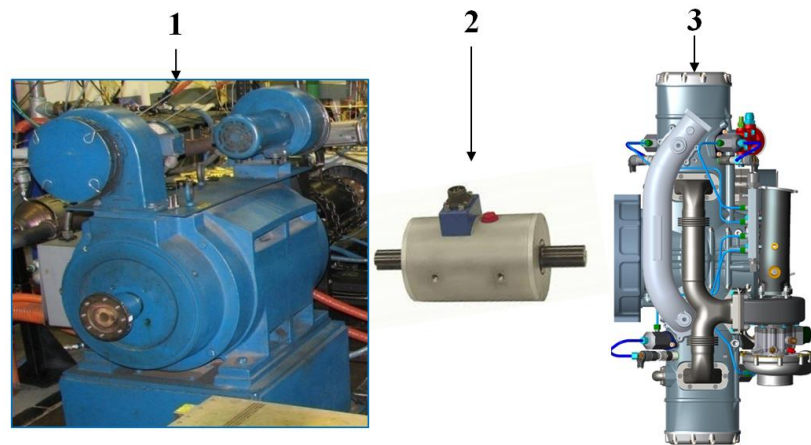


Figure 2. The scheme of the test bench and of the Eaton Lebow torque transducer: 1—Eaton AC electric engine break (300 kW, 8000 rpm); 2—Torque transducer Eaton Lebow (1000 Nm); 3—EM100D engine.

In order to meet all the testing requirements of the EM100D engine, the test bench was equipped with an intake air filtering and conditioning system (water cooled intercooler), an exhaust pressure conditioning system to simulate the counter pressure in the gas exhaust system, a system for the conditioning of the cooling liquid's temperature and for the engine oil, and a system to supply the high-pressure pump with fuel. Additionally, because the EM100D engine is designed with a dry oil pan, the test bench was provided with an oil tank equipped with a crankcase gas recirculation and filtration system.

The measurement of the air flow through the engine was carried out with a Meriam MTD500 type flowmeter with laminar current. The fuel flow was measured using a Pierburg PLU131-150 flowmeter produced by the AVL company (Perth, Australia).

The oil flow and the cooling liquid flow was measured with the use of Hedland flowmeters for oil and a 1100 series Blanchett flowmeter for the cooling liquid.

The Hedland oil flowmeter is a totally integrated control, acquisition, and data processing system with electronic display. It is equipped with a specific density compensation system for different types of oil.

The flowmeter for the measurement of the cooling liquid's flow has an accuracy and a repeatability of $\pm 1\%$ and a functioning temperature interval between $-100\text{ }^{\circ}\text{C}$ and $+177\text{ }^{\circ}\text{C}$.

The measurement of the engine speed was realized by using an RPM transducer mounted in the front part of the engine, in the extension of the crankshaft, while the turbocharger speed was measured with a PICOTURN-SM type RPM transducer combined with an electronic control device PICOTURN-BM.

The electronic management of the engine is ensured by a BOSCH CRS100 ECU, modified to permit the use of two injectors for each cylinder, that will be capable of injecting concomitantly, having the same injection law at each complete rotation of the crankshaft for each cylinder.

The schematic of the data acquisition and processing system used during the testing of the EM100D engine on the test bench is presented in Figure 3.

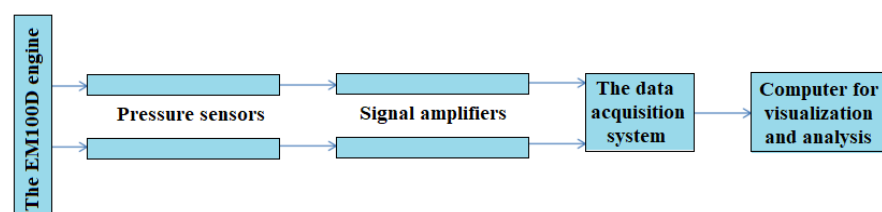


Figure 3. The scheme of the data acquisition and processing system.

The used pressure sensors are divided into two categories: sensors to measure static pressure and sensors to measure dynamic pressure (instantaneous). To acquire the value of the pressure inside the cylinders, inside the intake manifold, inside the exhaust manifold, and around the intake and the exhaust ports, dynamic pressure sensors were used. For the acquisition of the pressures before and after the turbocharger, in the crankshaft case, as well as at the entrance and the exit zones of the intake and of the exhaust manifolds, sensors for static pressure were used. The Kistler 6043A60 sensor for the determination of the pressure inside the cylinder is presented in Table 1.

Table 1. Measurement devices used in the experimental research.

Device Image	Name
	Kistler 6043A60 sensor for dynamic pressure
 <p style="text-align: center;">a. b.</p>	(a) The Kistler pressure sensor 7061b1; (b) The Kistler pressure sensor 4043
	The AVL 415SE smoke meter
	The Horiba exsa 1500 gas analyzer

The measurement of the pressure in the intake and the exhaust manifold was realized by using the sensor Kistler 7061B1 for the exhaust manifold shown in Table 1, being a water-cooled sensor, and sensor Kistler 4043A for the intake manifold, also presented in Table 1. The signal from the pressure sensors was picked up by the Kistler 5015A type signal amplifier.

The equipment with which a part of the experimental data was acquired is an AVL Indimodul type. The parameterization, the display, and the evaluation of the experimental

data were achieved by using the AVL IndiCom software. The experimental data acquired by the data acquisition system were transmitted to the computer's system to visualize and control the engine's testing process.

The ecological characteristics of the engine were determined by using specialized equipment that analyzed the chemical composition of the exhaust gases of the EM100D engine. The scheme of the exhaust gases analysis system is presented in Figure 4.

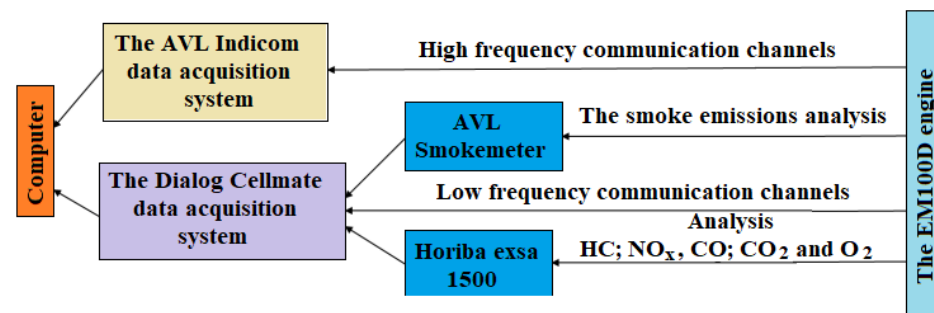


Figure 4. The scheme of the exhaust gases analysis system.

The analysis of the smoke emissions was realized with the AVL 415SE type smoke meter. The results were analyzed with a microprocessor, and the determined value was the filter smoke number (FSN). The AVL 415SE smoke meter is presented in Table 1. The analysis of the other pollutant emissions, hydrocarbons (HC), nitrogen oxides (NO_x), carbon mono oxide (CO), and carbon dioxide (CO_2), and the oxygen emission (O_2) were realized by using a Horiba exsa type gas analyzer, presented in Table 1.

The purpose of the research was to identify and to investigate a constructive, energy-efficient solution of a combustion chamber that would enable the EM100D engine to approach the engine program targets ($\text{NO}_x < 3.5 \text{ g/kWh}$, $\text{FSN} < 1.0$, $\text{bsfc} < 198 \text{ g/kWh}$). In order to achieve this goal, the experimental part consists of the development and the optimization of the combustion chamber's geometry, to establish the ecological and the energy performances of the engine.

Three shapes of the combustion chamber were investigated, in the following order:

1. Chamber 1—ovoid shape (lenticular);
2. Chamber 2—"butterfly" shape;
3. Chamber 3—toroidal shape.

The engine testing strategy for all three shapes of the combustion chamber that were mentioned above consists of the calibration of the engine for all the points mentioned in Figure 5 and in Table 2, in steady state conditions, to obtain the lowest specific fuel consumption. The testing points adapted to the EM100D engine considering the power curves, the torque, and the rotational speed are presented in Figure 5.

In the first phase, the engine was assembled to perform the testing with the combustion chamber 1 in the points indicated by the US-13 Mode testing cycle.

The obtaining of the minimum possible value of the effective fuel consumption for a certain point was realized by modifying the injection parameters: injection pressure, start of injection, injection strategy (pilot injection, post injection, pre-injection), and percentage of the turbocharger's electric assistance. In the moment in which the minimum value of the specific fuel consumption was reached, the parameters of the injection were modified again, in such a way that the smoke and the nitrogen oxides emissions should decrease in the respective order, without a specific fuel consumption penalty.

After the calibration of all the points from Figure 5 with chamber 1, the results were registered. After that, the engine was disassembled and went to the implementation of the second and third configuration of combustion chamber, respectively, following the same strategy as the one used for chamber 1. The geometry of the combustion chamber was designed so as to affect the shape of the piston that controls the intake ports as little as possible.

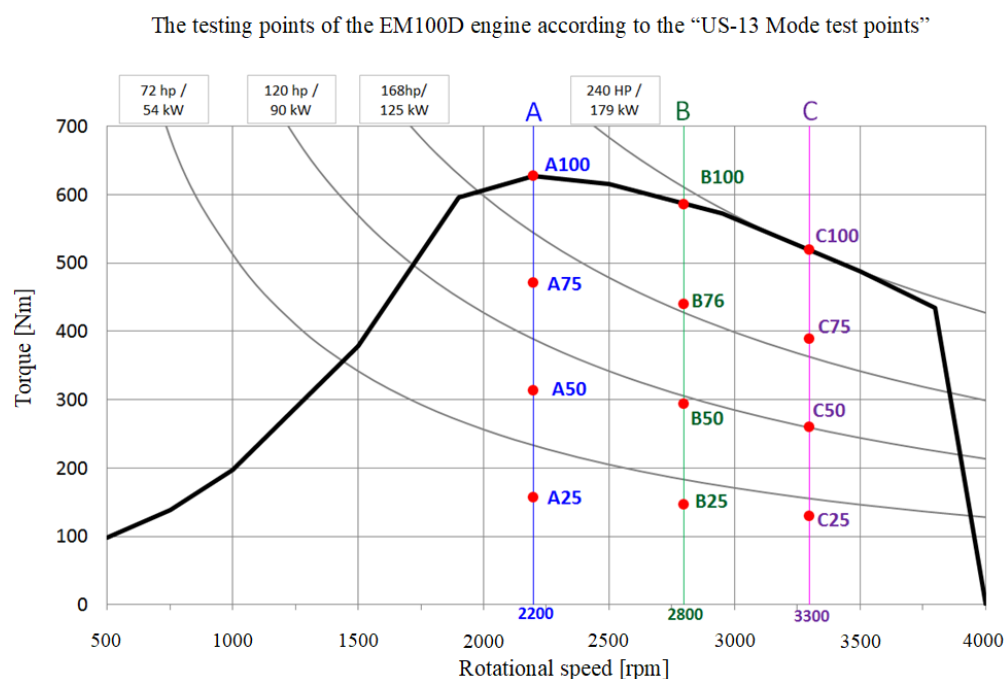


Figure 5. The testing points of the EM100D engine.

Table 2. The engine’s parameters in the testing points for US-13 Mode testing cycle.

Testing Point	Rotational Speed [rpm]	Power [kw]	Torque [Nm]
A100	2200	144	627
A75	2200	108	470
A50	2200	72	314
A25	2200	36	157
B25	2800	73	147
B50	2800	86	293
B75	2800	129	440
B100	2800	172	586
C100	3300	180	520
C75	3300	135	390
C50	3300	90	260
C25	3300	45	130

During the research for the development of the combustion chambers, the conclusion was that the optimization of their geometry requires more deeper research regarding the injection process and the role of the air swirl in the mixture formation. Therefore, after a first phase in which the ovoid (lenticular) chamber was tested on the engine, it was decided to design and manufacture a transparent combustion chamber, also able to generate an air swirl motion with different rotational speed. This would enable the study of the impact of swirl values on fuel jet development (penetration, dispersion, shape) and mixture formation in an environment that simulates the real conditions from the engine as closely as possible. The algorithm for the development of an optimal geometry of the combustion chamber is presented in detail in Figure 6.

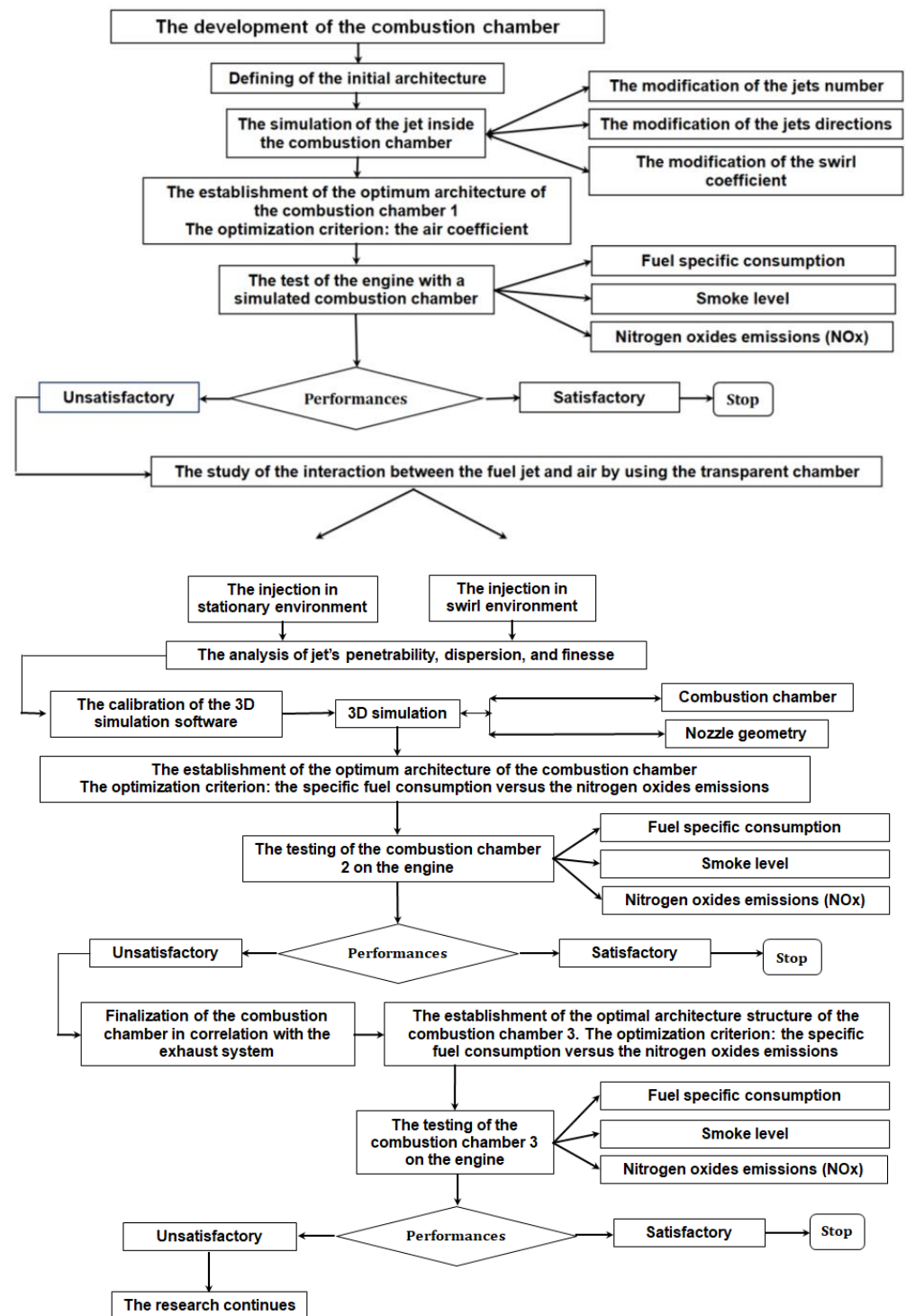


Figure 6. The research scheme for the combustion chambers.

The research started with the establishment of the combustion chamber 1 geometry (ovoid shape), having a volume of 60 cm^3 , to which an injection system with two injectors for one chamber was associated, as presented in Figure 7. As shown in Figure 7, the main zone of the combustion chamber is realized in the piston that controls the opening and closing of the exhaust ports (exhaust piston), and the injectors are diametrically disposed. The fuel jets delivered by the two injectors are interpenetrating.

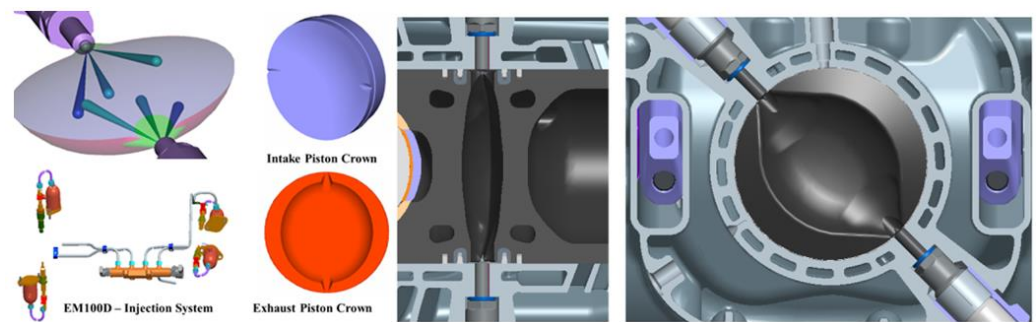


Figure 7. The ovoid combustion chamber.

According to the experimental research algorithm, the combustion chamber 1 was installed on the EM100D engine, and the following parameters were determined on the test bench: the fuel specific consumption and the level of smoke and nitrogen oxides emissions. The testing conditions were imposed by the testing cycle US-13 Mode HD test points. The measurement points, according to this testing cycle, are presented in Figure 8.

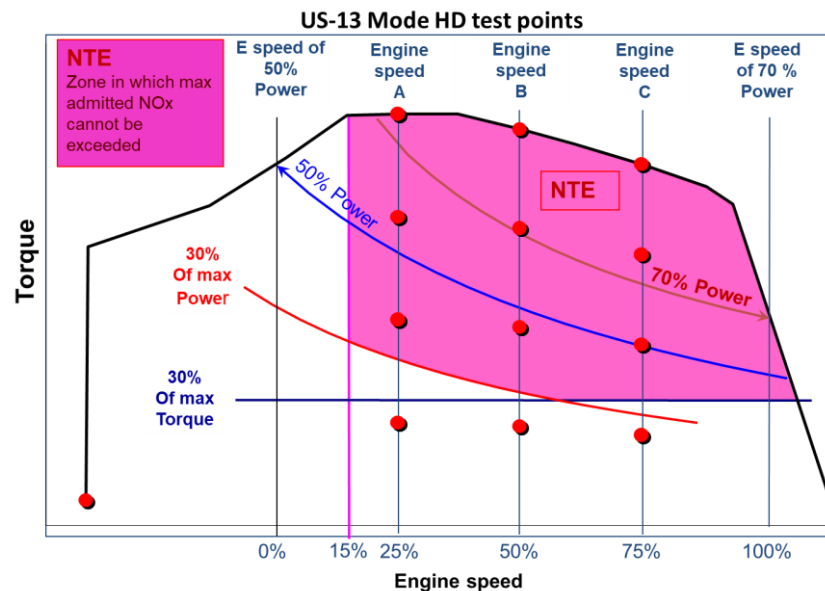


Figure 8. The testing cycle in 13 points (US-13 Mode HD test points).

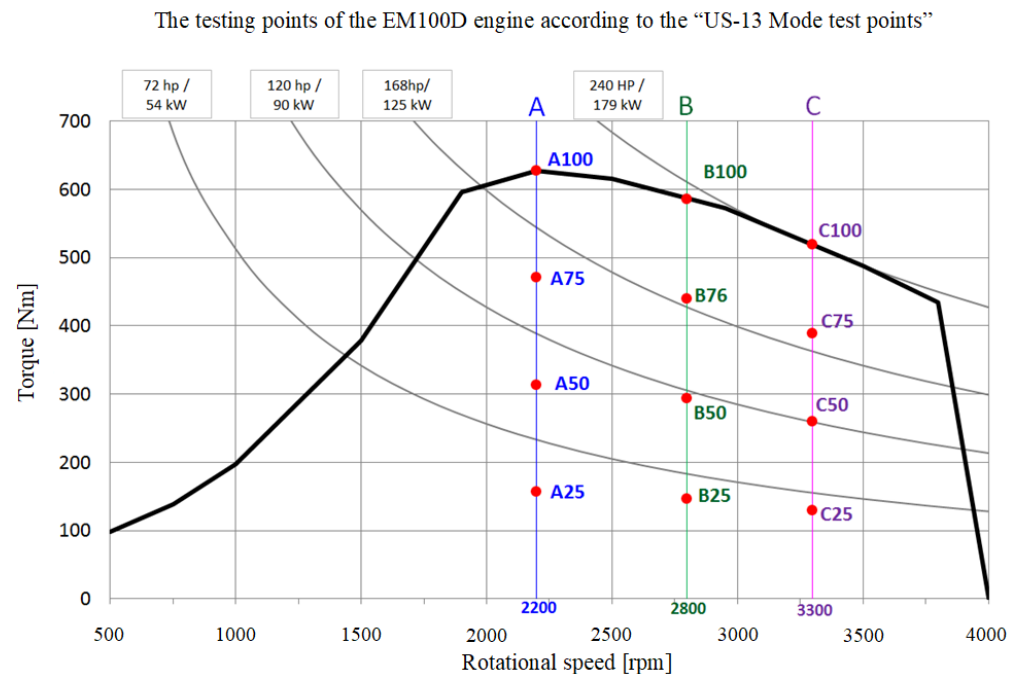
It can be observed that the maximum value of the air utilization coefficient was obtained for the conditions specified in the fifth row of Table 3 at: the injection advance 20 CA (crankshaft angle); the injection duration 13.5 CA; the swirl number 1; the injected flow $500 \text{ cm}^3/30 \text{ s}$; the orifice diameter 0.229. According to the adopted optimization criterion, this is the optimal variant of combustion chamber 1, as it results from Figure 9.

The target values for engine performance in terms of NO_x , smoke, and fuel consumption were presented above, and these are based on Euro IV emission regulations. These target values, once met, offer the possibility that the engine can be equipped relatively easily with an exhaust gases post treatment system in order to fulfill the conditions imposed by the EURO VI regulations in the moment in which the EM100D engine should equip buses and trucks.

The efforts made to improve the engine's performances equipped with the combustion chamber 1 were not successful on the entire engine map, so the next step was activated according to the research program plan, shown in Figure 6. In this step, the fuel spray formation and its interaction with the air inside of a transparent combustion chamber was studied.

Table 3. The engine's parameters in the testing points for US-13 Mode testing cycle for the combustion chamber 1 (ovoid shape).

Curr. No.	Injection Advance	Injection Duration	Swirl Number	Injected Flow	Orifice Diameter
	[CA]	[CA]		[cm ³ /30 s]	[mm]
1	20	13.5	0.5	320	0.183
2	20	13.5	1	320	0.183
3	20	13.5	2	320	0.183
4	20	13.5	0.5	500	0.229
5	20	13.5	1	500	0.229
6	20	13.5	2	500	0.229
7	10	8.64	1	320	0.183
8	10	8.64	2	320	0.183
9	10	8.64	1	500	0.229
10	10	8.64	2	500	0.229

**Figure 9.** The variation of the air utilization coefficient in the simulation conditions for the combustion chamber 1 (ovoid shape).

The next step was the constructive–functional optimization of the combustion chamber 1 (ovoid shape) by using a simulation of the fuel jet inside the combustion chamber, to establish its influence on the air utilization coefficient, which is the optimization criterion, as shown in Figure 9. The air utilization coefficient is the ratio between the air molecule number that reacts with the fuel jet and the total air molecule number situated inside the combustion chamber. The simulation conditions were modified by the variation in the number of jets, in the jets' directions, and in the swirl coefficient. The simulation of the jets' evolution was carried out using the Fluent program. In the first step, the 3D model was imported into the CFD software, after which the analysis was divided into the main characteristic components: intake, exhaust, active volume, and nozzle area. These areas were used to define the boundary conditions. Based on the geometric model, the finite volume model was realized by discretization. An important aspect in the analysis process is the size of the cells. Their size influences the calculation time and the accuracy of the results. For a higher calculation precision, a large number of elements would be necessary, but this would lead to an increase in the calculation time. In order to achieve a balance between

the simulation time and its accuracy, it is necessary to perform multiple simulations. The discretization was made by areas of interest, depending on their size and complexity. For one of the simulations, the mesh was generated based on the following parameters: cell size = 0.0015 and 9.375×10^{-5} ; closure level = 2; number of boundary layers = 1; number of domains = 1. In addition to these parameters, it was possible and necessary to define some initial parameters of the simulation conditions (e.g., speed and turbulence of fluid). This mathematical model was developed in order to be used in further research. This model was calibrated by using the experimental results. The simulation conditions are presented in Table 3.

The density of the air that the fuel is injected into has a great influence on the jet's penetration and atomization. Therefore, the research was carried out in different conditions for the pressure and the temperature inside a transparent (optical) combustion chamber that should enable the visualization of the fuel spray formation and development in a steady state (motionless environment) based on different injection pressures and orifice diameters as a first step, and then the fuel sprays' interaction with the air being in a rotational motion (swirl motion) inside of the chamber as a second step. The first step would give an indication on the con angle of the fuel jet, its dispersion, and penetration based on different injection pressures and nozzle orifice diameters. The second step would give information on the effect of the swirl motion on the fuel jets' direction and their interaction with each other. This information would be useful to calibrate the simulation model for future combustion chambers architecture trials. The main parameter that influences the spray penetration, beside the density of the air it is injected into, if the same amount of fuel is injected at different pressures, is the injection duration. Therefore, experiments were carried out at different injection pressures and durations.

An OPOC optical combustion chamber that matched the architecture of the EM100D combustion chamber 1 (ovoid shape) as closely as possible was designed and manufactured. This chamber is comprised of a steel frame on which two injectors, a pressure sensor, and a thermocouple can be installed. The steel frame allows the installation of two components that depict the shape of intake and exhaust pistons and two quartz glasses that close the chamber volume. The steel frame has a flange that can be connected to other chambers or devices in order to enable the generation of air motion inside the chamber as presented in Figure 10.

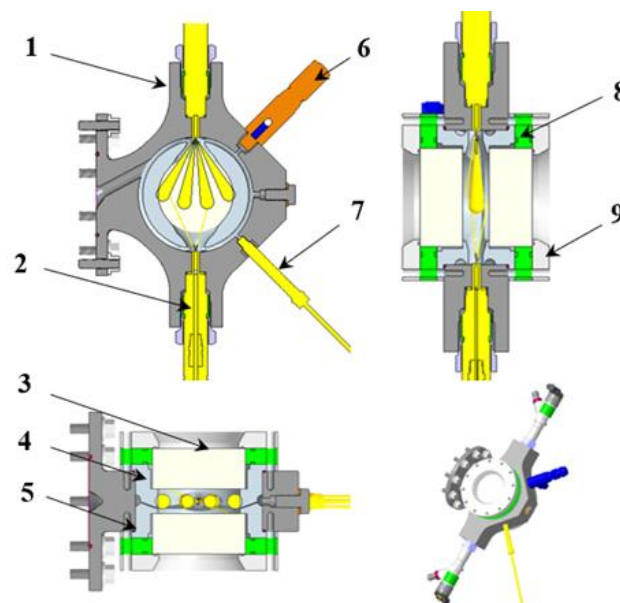


Figure 10. OPOC optical combustion chamber: 1—Steel frame; 2—Injector; 3—Quartz glass; 4—Exhaust piston cap; 5—Intake piston cap; 6—Safety valve; 7—Dynamic pressure sensor; 8—Sealing plate; 9—Closing cap.

A preheating chamber was designed and manufactured as well in order to help increase the temperature of the air entering the optical chamber as shown in Figure 11. Controlling temperature would enable the study of the effect of different temperatures on the fuel sprays' formation and on the process of the start of combustion.

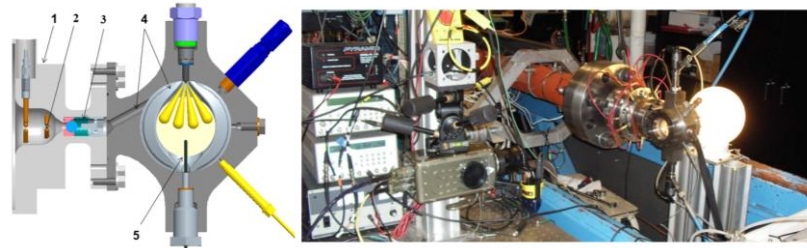


Figure 11. Preheating chamber and OPOC optical combustion chamber assembly: 1—Preheating chamber case; 2—Glow plug; 3—One-way valve; 4—Tangential channel for the swirl generation; 5—Temperature sensor.

The preheating chamber allows the installation of up to 10 glow plugs that can be controlled individually in order to influence and control the overall air temperature entering the transparent combustion chamber. In order to generate the air motion inside of the transparent combustion chamber, a separate pilot ignition combustion chamber was used (Figure 12). The pilot ignition chamber was modified from an existing optical combustion chamber by installing a spark plug instead of the injector.

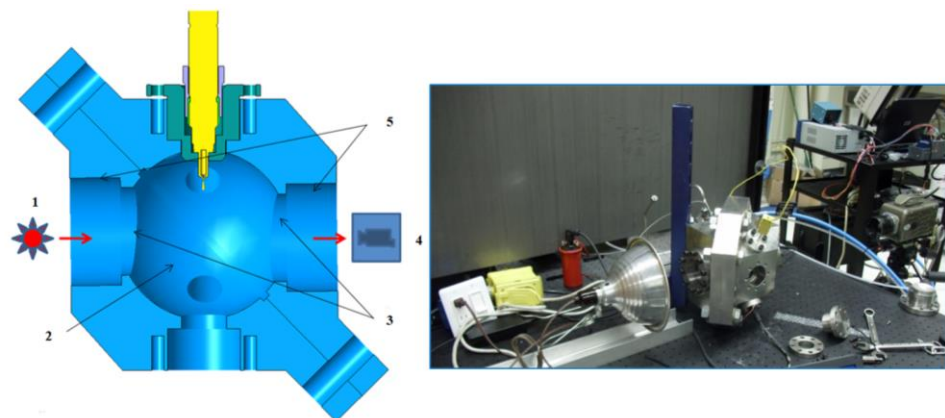


Figure 12. Pilot ignition optical chamber, diameter fused silica plugging windows: 1—Light source; 2—Spherical combustion chamber; 3—Visualization chambers; 4—High speed video camera; 5—Transparent chambers.

The combination of the three chambers (the pilot ignition optical chamber, the preheating chamber, and the OPOC combustion chamber) is shown in Figure 13 together with the injector nozzle orifice configuration that was used in this test. By combining the two combustion chambers, an assembly was realized that allowed the obtaining of some pressures and temperatures, as well as the values of the swirl movement, close to those registered for the EM100D engine during its functioning. This assembly was called transparent chamber with swirl environment, shown in Figure 13.

The swirl chamber ensures the individual pressurization of the two chambers at different values because of the one-way valve placed between the two mounting flanges, a valve that permits a gas transfer between the two chambers but only from the stationary chamber to the swirl medium chamber. Additionally, the chemical composition of the gases in the two chambers can be different.

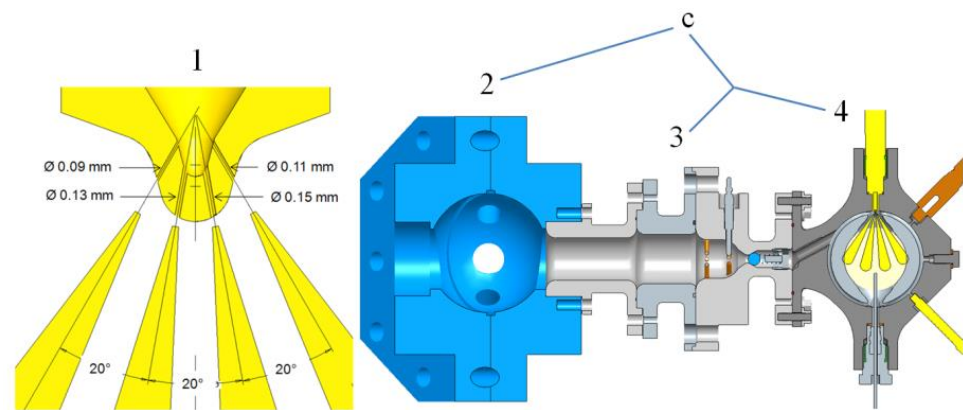


Figure 13. The swirl chamber assembly obtained by the combination of the pilot ignition optical chamber, the preheating chamber, and the OPOC combustion chamber: 1—Custom injector used for spray characterization; 2—Pilot ignition experimental combustion chamber; 3—Preheating chamber; 4—Transparent stationary combustion chamber.

These can be separately supplied from different gas bottles. In this situation, the combustion chamber with the swirl environment can be pressurized with an inert gas (nitrogen or air), depending on the performed test, while the chamber with a stationary environment can be pressured with a fuel mixture of nitrogen, oxygen, and methane in different concentrations, a mixture with which combustion can be initialized by the spark of a plug mounted in the place of the injector. As long as the pressure inside the swirl chamber is higher than the one inside the stationary medium chamber, the mass transfer between the chambers is interrupted by the one-way valve. In the moment in which the fuel mixture is ignited, the pressure and the temperature rise, exceeding the pressure inside the swirl environment chamber. The mass transfer between the two chambers is quickly initialized by the opening of the one-way valve, generating a swirl movement because of the tangential channels through which the burning products from the stationary chamber enter the chamber with a swirl environment.

By using the transparent chambers, studies were realized regarding the interaction between the injected jets and the injection environment found both in the stationary state and in a swirl movement. The jets' penetrability, dispersion, and finesse were studied, and it was possible to appreciate the homogenization process of the fuel mixture. In Figures 14 and 15, the injected fuel jets in stationary medium and in swirl medium at a rotational speed of 2500 rpm at four time intervals after the start of injection at the same counter pressure and at the same injection pressure are presented. The transparent chamber offered the possibility of visualizing the initialization and the progress of the combustion process, as is presented in Figure 16.

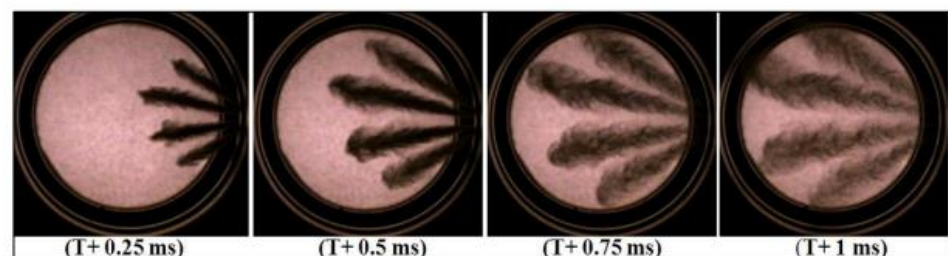


Figure 14. Images taken in the stationary environment chamber.

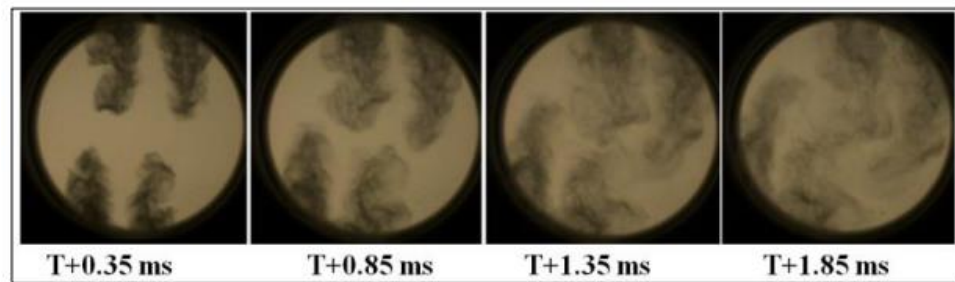


Figure 15. Images taken in the swirl environment chamber.

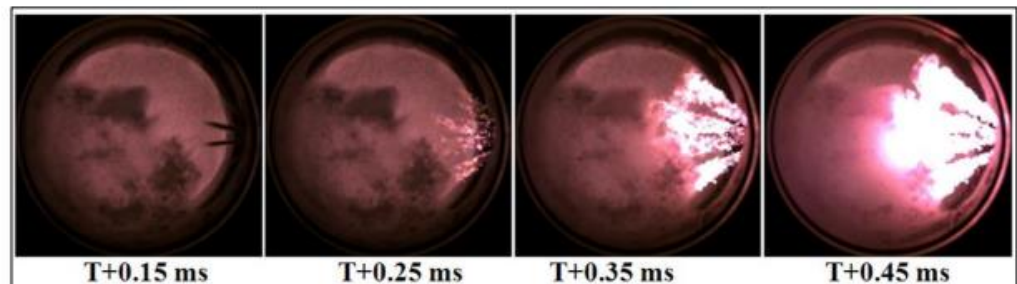


Figure 16. The initialization of the ignition and the displacement of the flame front in the chamber with a stationary environment.

The images presented in Figure 16 were taken in the stationary environment in the following conditions: the injection pressure 1000 bar, the counterpressure in the transparent chamber 23 bar, the temperature of the environment in which the injection took place 800 °C, and the injection duration 0.23 ms. In Figure 17, the ignition and the displacement of the flame front process in the following conditions are presented: the injection in a swirl environment with the rotational speed 6000 rpm, the injection pressure 1500 bar, the counterpressure in the transparent chamber 20 bar, and the injection duration 0.5 ms.

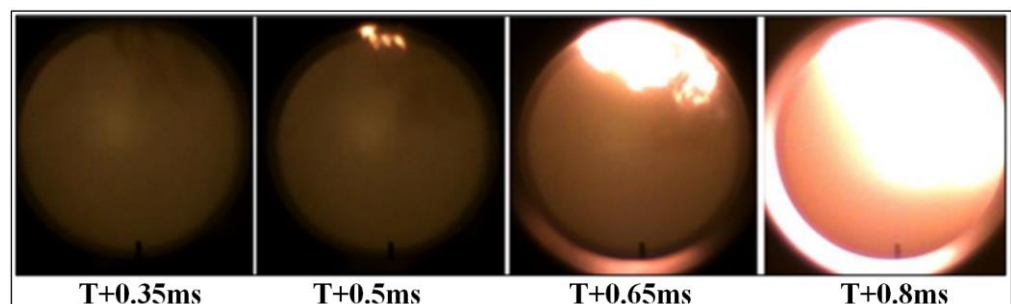


Figure 17. The initialization of the ignition and the displacement of the flame front in the chamber with a swirl environment.

The combustion chamber 2, designed with a more complex form, named “butterfly”, has the same volume of 60 cm³, maintaining the same engine compression ratio. The constructive–functional optimization was made in the virtual environment using the Fluent program. The modified input data were the injection pressure, the counterpressure, the state of the environment in which the injection took place (stationary or with various rotational speeds of the swirl), the temperature of the injection’s environment, the diameter of the nozzle’s pulverization orifices, and their orientation. The model to be analyzed was calibrated by using the experimental data obtained through the visualization of the injection and the mixture formation processes inside the transparent chambers.

The optimization criterion for the burning chamber 2 was the variation in the specific fuel consumption values depending on the NO_x emissions, at various values of the swirl

rotational speeds. In Figure 18, the combustion chamber 2 geometry (butterfly shape) is presented, the realization of the butterfly shape being made in the exhaust piston. The evolution of the chamber's optimization criterion values in a virtual environment is also presented, observing that the indicated specific fuel consumption depending on the indicated NO_x emission is most favorable for a swirl movement with the swirl number 2 (the rotational speed of the injection environment is two times bigger than the engine's rotational speed). The swirl number represents the ratio between the air rotational speed and the engine's rotational speed. The research was conducted at various air rotational speeds. For this optimal situation, in Figure 18, the development in time of the injection process, the initialization of the combustion, and the evolution of the flame front are also presented.

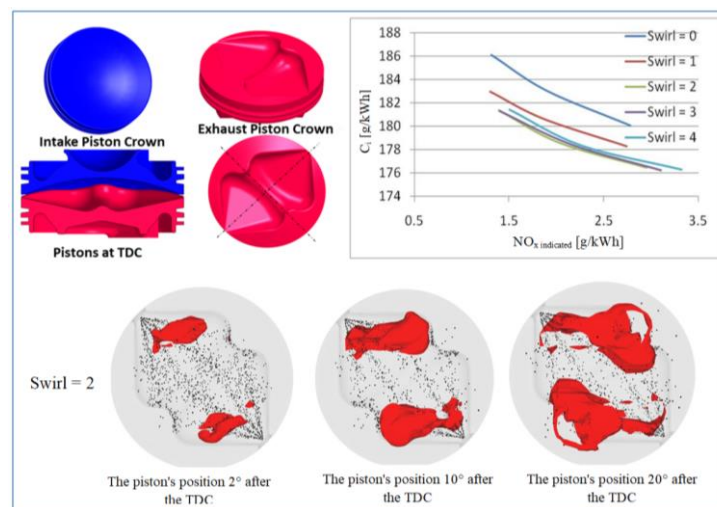


Figure 18. The combustion chamber 2 (butterfly shape) and its performances in virtual environment.

The practically realized combustion chamber 2 was mounted on the EM100D engine, through which tests on the bench were carried out, according to the testing cycle US-13 Mode HD test points, as presented in Figure 9. The architecture of the combustion chamber 3 was designed in such way as to use the swirl movement in the pulverization of the fuel jet and in the occupation of the entire space inside the combustion chamber with pulverized fuel. From previous research, the existence of some difficulties in the occupation of the combustion chamber's center by the injected fuel were observed. As a result, in the construction of the combustion chamber 3 (toroidal shape), the existence of a central "dome" was chosen that has the role of dislocating the volume from the center of the chamber and contributing to the generation of a "tumble" movement of the air inside the burning chamber. Therefore, the shape of the combustion chamber 3 was designed in the form of torus, the fuel jets being injected in the direction of the swirl movement.

In Figure 19, the geometry of the torus shape chamber is presented, observing that, this time, the shape of the burning chamber was machined both in the head of the intake piston and in the head of the exhaust piston. The mechanical processing of a part of the intake piston does not have a major influence on the scavenging process because the central dome occupies a relatively small part of the combustion chamber. The shape of the surface at the periphery of the combustion chamber remained suitable for the entrance of the fresh air into the cylinder. The volume of the combustion chamber 3 was also maintained at 60 cm^3 , to keep the engine's compression ratio.

The same as in the combustion chamber 2, the optimization criterion for the burning chamber 3 was the dependence between the value of the fuel specific consumption and the NO_x emission, at various values of the swirl rotational speed. This dependence is also presented in Figure 19. It can be observed that the most favorable dependence between the fuel specific indicated consumption " c_i " and the NO_x emissions is realized when the value

of the swirl movement coefficient is five, much greater than in the case of the combustion chamber 2. Additionally, in Figure 19, the development of the injection process in time, the combustion initialization, and the combustion evolution for the situation in which the swirl coefficient is four are presented, considering that a greater value of the swirl will affect the gas exchange process.

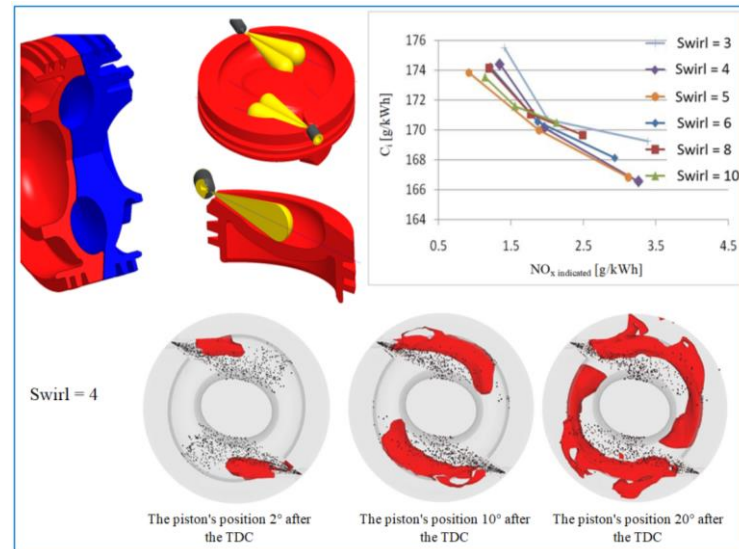


Figure 19. The combustion chamber 3 (toroidal shape) and its performances in virtual environment.

After the simulation, an improvement in this combustion chamber's performances regarding the performance criterion was observed, compared to the combustion chamber 2. This led to the practical realization of this chamber and its testing on the EM100D engine, also according to testing cycle US-13 Mode HD test points.

3. Results

Considering the results obtained from the analysis of the fundamental processes, the three types of the combustion chambers were realized. Further, the energetic and the ecological results experimentally obtained are presented in synthesis.

As mentioned before, the combustion chamber 1 has the lenticular form as its constructive principle, being provided with two injectors. In Figure 20, the evolution of the specific fuel consumption of the engine that is equipped with the combustion chamber 1 is presented.

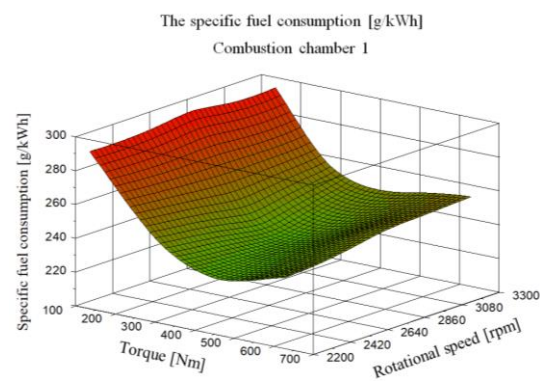


Figure 20. The specific fuel consumption of the engine equipped with the combustion chamber 1.

From Figure 20, a stable evolution of the engine on the entire testing domain was found, with minimum values of the specific fuel consumption approximately halfway through the maximum load and an approximately constant evolution of the specific fuel

consumption depending on the rotational speed, with a moderate rise for the rotational speeds at the ends of the functioning interval. In Figure 21, the evolution of the nitrogen oxides specific emissions for the combustion chamber 1 is presented. A quick growth in the nitrogen oxides emissions is observed at high loads due, in particular, to the high combustion temperatures.

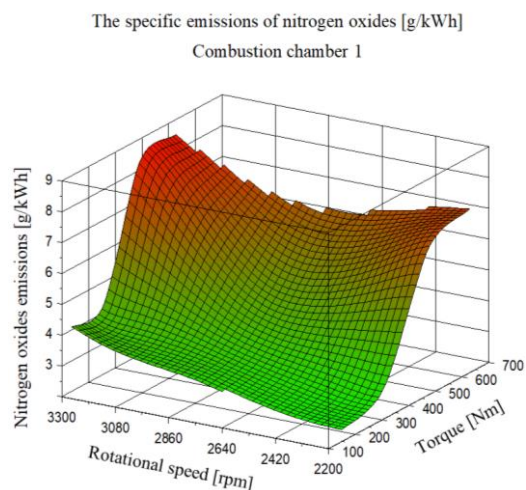


Figure 21. The nitrogen oxides specific emissions for the engine equipped with the combustion chamber 1.

In Figure 22, the evolution of the smoke emission for the combustion chamber 1 is presented. This has an irregular distribution on the engine's functioning domain, which is likely due to the different vortex with pronounced swirls formed in the circular movement, perpendicular to the cylinder's axis. The greater fuel quantity injected at high loads also leads to superior smoke emissions.

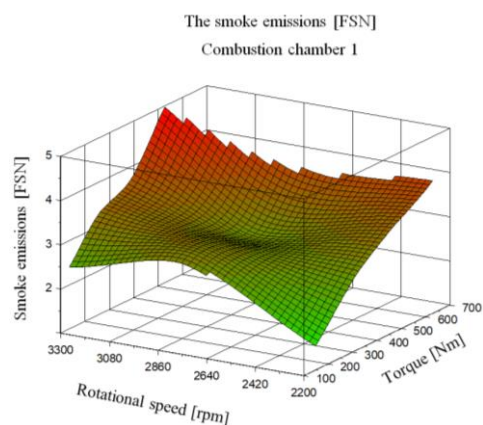


Figure 22. The smoke emission of the engine equipped with the combustion chamber 1.

The second type of combustion chamber studied (chamber 2) has the butterfly shape as its constructive principle. In Figures 23–25, the evolutions of the specific fuel consumption, of the nitrogen oxides specific emissions, and of the smoke emissions for this chamber are presented in spatial diagram.

From Figure 23, a stable evolution of the engine on the testing domain can be observed, with minimum values of the specific fuel consumption at approximately 30% of the maximum load and an approximately constant evolution depending on the rotational speed, with a moderate rise for the rotational speeds at the ends of the functioning interval.

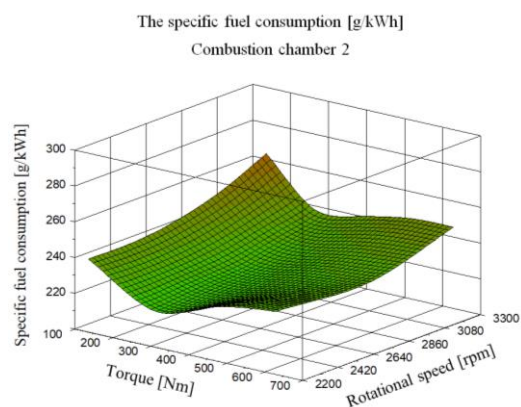


Figure 23. The specific fuel consumption for the engine equipped with the combustion chamber 2.

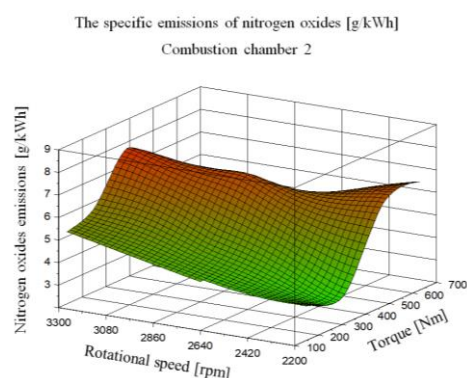


Figure 24. The nitrogen oxides emission of the engine equipped with the combustion chamber 2.

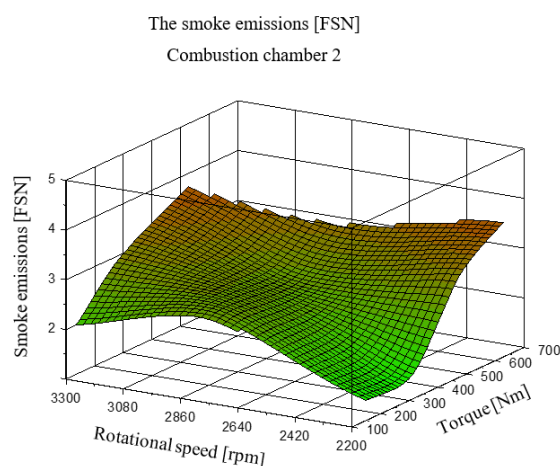


Figure 25. The smoke emission of the engine equipped with the combustion chamber 2.

From Figure 24, it is found that the maximum nitrogen oxides emissions values are registered in the domain of high loads, and they grow constantly as the rotational speed rises.

The evolution of the smoke emission has an irregular distribution on the engine's functioning domain, with local maximums at high rotational speeds and loads, at medium rotational speeds and low loads, and at low rotational speeds and high loads, evolution that suggests the correlation with the movement of the working fluid in the cylinder is less favorable at low rotational speeds, but too intense at high rotational speeds, as shown in Figure 25. The third type of combustion chamber is based on the toroid structure of its geometry. In Figures 26–28, the evolutions of the specific fuel consumption, of the nitrogen

oxides specific emissions and of the smoke emissions for this chamber are presented in the same type of spatial diagrams.

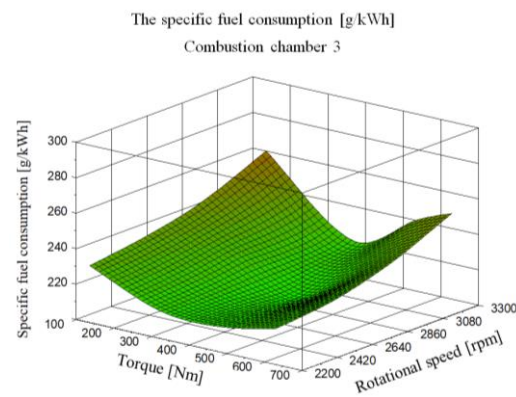


Figure 26. The specific fuel consumption for the engine equipped with the combustion chamber 3.

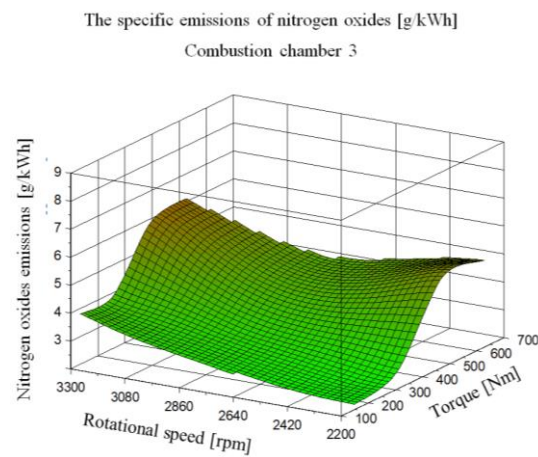


Figure 27. The nitrogen oxides emission of the engine equipped with the combustion chamber 3.

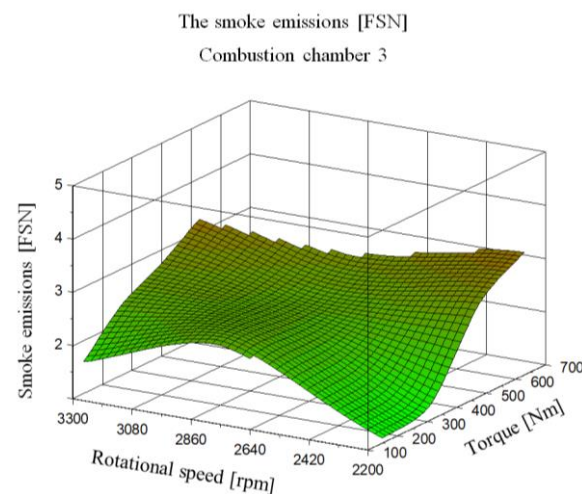


Figure 28. The smoke emission of the engine equipped with the combustion chamber 3.

In Figure 26, a stable evolution of the engine on the entire testing domain can be observed, with minimum values of the specific fuel consumption approximately halfway through the maximum load and an approximately constant evolution of the specific fuel consumption depending on the rotational speed, with a moderate rise for the rotational speeds at the ends of the functioning interval. Compared with the evolution of the other

combustion chambers, an accentuation of the fuel consumption to superior levels at the ends of the testing interval can be found.

In Figure 27, a quick rise in the nitrogen oxides at high loads can be observed due, in particular, to the high combustion temperatures. A constant rise in the emissions depending on the rotational speed at low loads and an evolution with a local minimum at high loads and medium rotational speeds is registered.

The evolution of the smoke emission (presented in Figure 28) has an irregular distribution on the engine's functioning domain, which is likely due to the different vortex with pronounced swirls formed in the circular movement, perpendicular to the cylinder's axis. The greater fuel quantity injected at high loads also leads to superior smoke emissions.

4. Discussion

The synthesis of the energetic and of the ecological parameters for the three constructive solutions of the combustion chambers, identified in the standardized test points, is presented in Figures 29–31.

The values of the energetic and ecological parameters determined for the three combustion chambers are synthetically presented in Table 4.

Table 4. The values of the energetic and ecological parameters determined for the three combustion chambers.

Testing Points	Rot. Speed	Torque	M.E.P.	Power	The Specific Fuel Consumption "c _e "			NOx			The Smoke Index		
					ch. 1	ch. 2	ch. 3	ch. 1	ch. 2	ch. 3	ch. 1	ch. 2	ch. 3
	[rpm]	[Nm]	[bar]	[kW]	[g/kWh]			[g/kWh]			[FSN]		
A100	2200	627	15.9	144	242	235	220	7.3	6.8	5.1	3.5	3.2	2.8
A75	2200	470	11.9	108	233	230	214	6.7	6.5	5.2	2.9	2.5	2.2
A50	2200	314	8.0	72	247	220	216	3.1	3.3	2.7	2.2	1.0	0.8
A25	2200	157	4.0	36	287	238	230	2.4	3.5	2.2	1.1	0.9	0.6
B25	2800	147	3.8	73	292	243	240	3.2	4.2	2.8	2.5	2.1	1.9
B50	2800	293	7.6	86	241	225	223	3.7	5.1	3.2	2.5	2.1	1.9
B75	2800	440	11.1	129	235	228	209	4.9	7.1	4.1	2.3	2.1	1.9
B100	2800	586	14.8	172	248	231	225	6.5	5.0	4.5	3.3	2.7	2.3
C100	3300	520	11.7	180	250	245	238	8.5	6.2	6.1	4.4	3.2	2.7
C75	3300	390	9.8	135	246	240	220	8.2	7.7	5.8	3.2	2.8	2.2
C50	3300	260	6.6	90	257	238	235	4.3	5.8	3.9	2.8	2.3	1.8
C25	3300	130	3.4	45	294	263	260	4.1	5.2	3.8	1.9	1.5	1.1

For the three combustion chambers experimentally studied, the results show that a toroid form combustion chamber ensures a superior behavior of the engine, in energetic and ecological aspects, with the specific fuel consumption being reduced by 11.5% compared to the combustion chamber 1 and by 9% compared to the combustion chamber 2. The nitrogen oxides emissions are reduced by 27% compared to the combustion chamber 1 and by 34% compared to the combustion chamber 2. The smoke emission is reduced by 47% compared to the combustion chamber 1 and by 19% compared to the combustion chamber 2. As a result of this study, a significant improvement in the engine's ecological parameters obtained by modifying the shape of the combustion chamber manufactured in the piston bowls can be observed.

In Figure 32, the comparison of the specific fuel consumption between the three variants is presented.

From Figure 32, the results show that that fuel consumption in the case of chamber 3 (toroidal shape) was reduced by up to 12.5% compared with the chamber 1 (ovoid shape) and up to 8% compared with the chamber 2 (butterfly shape).

In Figure 33, the comparison between the mean nitrogen oxides and smoke emissions for the three combustion chambers is presented.

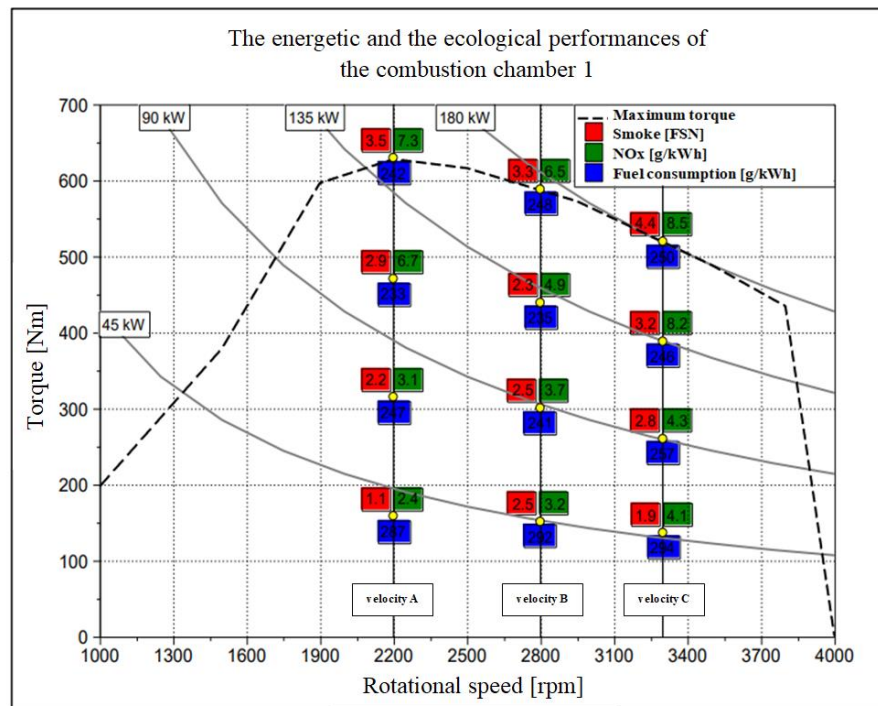


Figure 29. The energetic and the ecological parameters of the engine equipped with the combustion chamber 1 (ovoid shape).

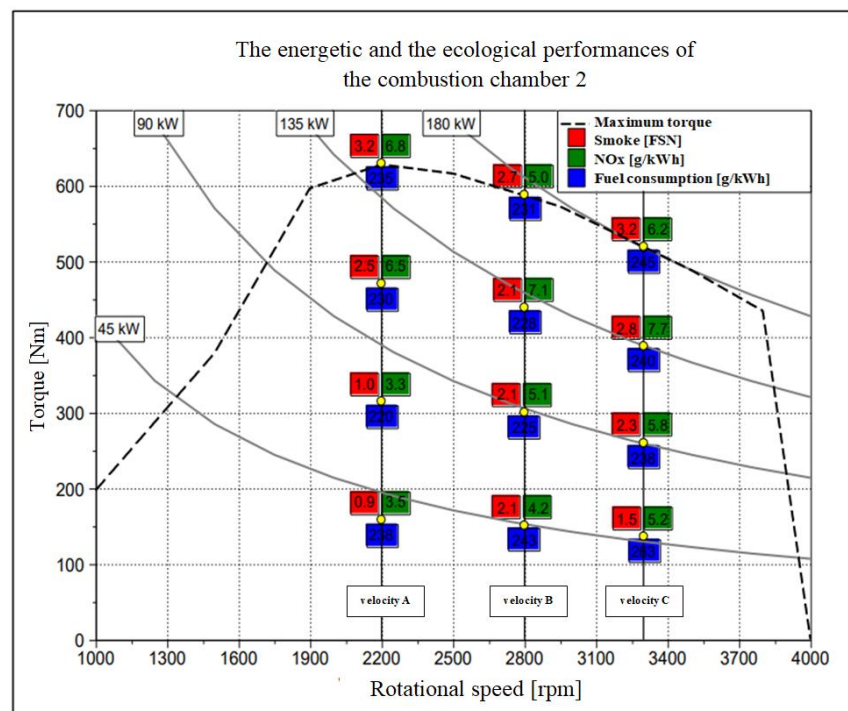


Figure 30. The energetic and the ecological parameters of the engine equipped with the combustion chamber 2 (butterfly shape).

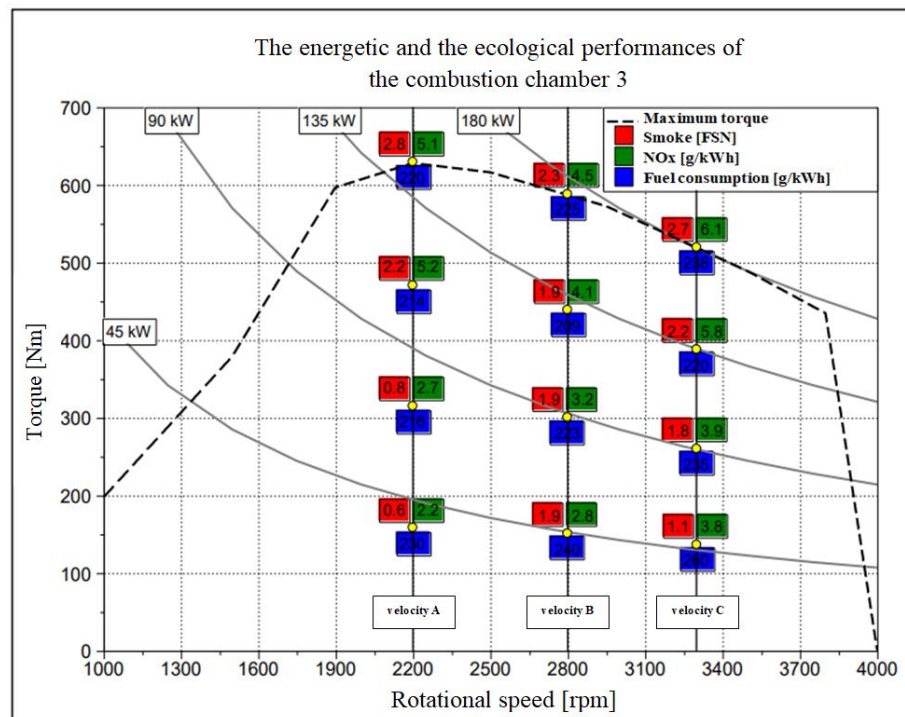


Figure 31. The energetic and the ecological parameters of the engine equipped with the combustion chamber 3 (toroidal shape).

The minimum specific fuel consumption comparison between the three combustion chambers

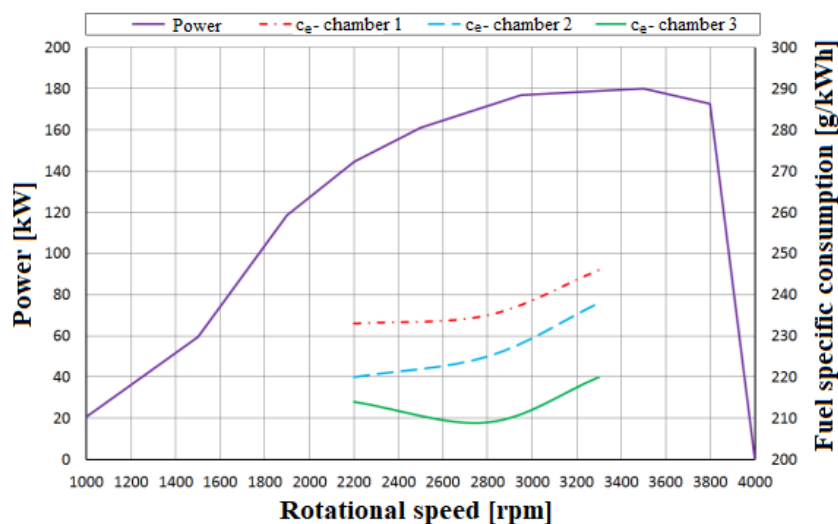


Figure 32. Comparison of the minimum fuel specific consumption between the three combustion chambers.

For the combustion chamber 1, from Figure 29 and Table 4, it is found that the NO_x emission has a maximum value of 8.5 g/kWh in the point C100 from Figure 5, corresponding to a rotational speed of 3000 rpm and an engine power of 179 kW. The maximum value of the smoke emission reaches its peak at 4.4, also in the point C100. The minimum fuel specific consumption of 233 g/kWh is registered in the point A75, shown in Figure 5, corresponding to a rotational speed of 3000 rpm and an engine power of 108 kW. In these conditions, it was appreciated that the functioning of the EM100D engine is unsatisfactory, so the research was moved to develop another combustion chamber, according to the scheme presented in Figure 6.

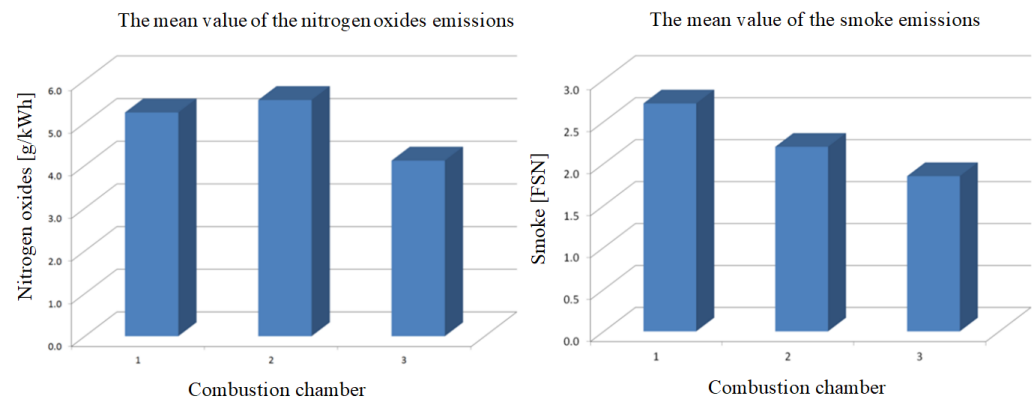


Figure 33. Comparison between the mean nitrogen oxides and smoke emissions for the three combustion chambers.

For the combustion chamber 2, from Figure 30 and Table 4, it is found that the NO_x emission has a maximum value of 7.7 g/kWh in the point C100 from Figure 5, corresponding to a rotational speed of 3000 rpm and an engine power of 179 kW. The maximum value of the smoke emission reaches its peak at 4.4, also in the point C100. The minimum fuel specific consumption of 233 g/kWh is registered in the point A75, shown in Figure 5, corresponding to a rotational speed of 3000 rpm and an engine power of 108 kW. In these conditions, it was appreciated that functioning of the EM100D is also unsatisfactory, so the research was moved to develop another combustion chamber, according to the scheme presented in Figure 6.

For the combustion chamber 3, from Figure 31 and Table 4, it was found that the nitrogen emission has a maximum value of 6.1 g/kWh in the point C100, the smoke emission reaches 2.8 FSN in the point A100, corresponding to a rotational speed of 2200 rpm and a power of 144 kW, and the minimum fuel consumption is 209 g/kWh in the point B75, corresponding to a rotational speed of 2800 rpm and a power of 129 kW.

From Table 4, it can be observed that the minimum values of the nitrogen oxides and smoke emissions are registered in the point A25, corresponding to a rotational speed of 2200 rpm and a power of 36 kW.

However, these results were not considered totally satisfactory, because the combustion chamber 3 does not totally fulfil, at the level of maximum demands, the conditions imposed by the initial target values.

The testing showed that usually, for an opposed piston engine, more than one injector per cylinder is required. This is imposed by the larger volume per cylinder, by the desire to have a reasonably small diameter of the nozzle's holes, and by the difficulty of placing a larger number of holes in the nozzle. To prevent the collision with the sprays generated by the other injector, the penetration of the fuel sprays must be short enough. It is recommended to use smaller hole diameters, since the jets' penetration and atomization strongly depend on this parameter. The duration of the fuel injection has a significant influence on the sprays' atomization and penetration, so more injection events will be beneficial. The fuel sprays can occupy the entire space of the combustion chamber even if there is no air motion inside the cylinder. For a good scavenging, the architecture of the combustion chamber must reduce the velocity of the rotational air movement and enhance local turbulence instead. A higher level of swirl will negatively affect the mixture formation.

During the research, it was observed that in the case of the combustion chamber 1 (ovoid shape) and of the combustion chamber 2 ("butterfly" shape), the sprays are affected, and the fuel does not reach the center of the cylinder. This is why the combustion chamber 3 (toroidal shape) was realized. It was observed that in this case, the combustion chamber was fully occupied by the fuel. Therefore, the energetic and the ecological performances for the combustion chamber 3 are much improved compared with the other variants. The

results of this research can be used for the further development of the OPOC engine. The mathematical model developed in this research was calibrated by using the results of the experiment. This calibrated model can be used for a further improvement of the engine's performances, reducing the time and the costs compared to experimental research.

Therefore, the research continued. As a result, a new engine with smaller dimensions was designed and realized. This will be subject of another scientific paper. Another research direction will be the improvement of the EM100D engine's performances in the case of using Diesel fuel. For this, the use of two injectors in the cylinder is necessary. It is important that the jets should not intersect, which is why it is important to adopt the multiple injections technique. It is possible to adopt the variant with fuel injection pressure over 2500 bar with multiple injections, which should ensure a limited penetration of the jets and a corresponding atomization. EGR techniques can be adopted to reduce the nitrogen oxides emissions. Within a project entitled "Water recovery system from vehicle's combustion engine exhaust gas", research was carried to recover the water vapors from the exhaust gases. This was a Cheques of Innovation project, and the project's code was PN-III-P2-2.1-CI-2018-1566. An important technique to reduce nitrogen oxides emissions is to lower the maximum temperature inside the cylinder. This can be realized by the injection of the recovered water in order to temper the maximum temperature of the engine cycle, so the nitrogen emissions should be diminished. Another research subject will be the use of gaseous fuels, such as methane and hydrogen, or of synthetic fuels.

This internal combustion engine with opposed pistons can be used in hybrid electric vehicles (HEV). As shown above, the minimum pollutant emissions of the EM100D engine are registered at low and medium loads, but the specific fuel consumption is higher. An internal combustion engine used in HEV has the advantage that it functions in a single regime, so its control is simpler. The functioning regime must be chosen in such a way as to achieve a compromise between the value of the fuel consumption and the level of the pollutant emissions.

Author Contributions: Conceptualization, A.T.; data curation, H.B., A.T., T.M. and F.B.S.; formal analysis, H.B., A.T., T.M. and F.B.S.; investigation, A.T.; methodology, A.T.; visualization, H.B., A.T., T.M. and F.B.S.; writing—original draft preparation, H.B., T.M. and F.B.S.; writing—review and editing, H.B., T.M. and F.B.S.; All authors have read and agreed to the published version of the manuscript.

Funding: This research was funded by the University of Oradea.

Data Availability Statement: Not applicable.

Conflicts of Interest: The authors declare no conflict of interest.

References

1. Statista. Available online: https://www.statista.com/topics/7476/transportation-emissions-worldwide/#topicHeader_wrapper (accessed on 16 November 2022).
2. Office for National Statistics. Available online: <https://www.ons.gov.uk/economy/environmentalaccounts/datasets/ukenvironmentalaccountsatmosphericemissionsroadtransportemissionsbypollutantunitedkingdom> (accessed on 20 November 2022).
3. European Views. Available online: <https://www.european-views.com/2022/11/eu-proposes-new-euro-7-standards-to-reduce-pollutant-emissions-from-vehicles/> (accessed on 20 November 2022).
4. European Environment Agency. Available online: <https://www.eea.europa.eu/data-and-maps/indicators/transport-emissions-of-air-pollutants-8/transport-emissions-of-air-pollutants-8> (accessed on 21 December 2022).
5. Hartung, S. Powertrains of the Future—How We Will Meet our Climate Goals through Technology Neutrality. In Proceedings of the 42nd International Vienna Motor Symposium, Vienna, Austria, 29–30 April 2021; ISBN 978-3-9504969-0-1.
6. Anselma, P.G.; Belingardi, G. Fuel cell electrified propulsion systems for long-haul heavy-duty trucks: Present and future cost-oriented sizing. *Appl. Energy* **2022**, *321*, 119354. [CrossRef]
7. Teixeira Rodrigues, C.; Lopes, G.F.; Alonso, C.G.; de Matos Jorge, L.M.; Paraíso, P.R. An autonomous fuel cell: Methanol and dimethyl ether steam reforming direct fed to fuel cell. *Int. J. Hydrog. Energy* **2023**, *48*, 4052–4063. [CrossRef]
8. Muthukumar, M.; Rengarajan, N.; Velliyangiri, B.; Omprakas, M.A.; Rohit, C.B.; Kartheek Raja, U. The development of fuel cell electric vehicles—A review. *Mater. Proc.* **2021**, *45*, 1181–1187. [CrossRef]

9. Longwic, R.; Sander, P.; Zdziennicka, A.; Szymczyk, K.; Janczuk, B. Combustion Process of Canola Oil and n-Hexane Mixtures in Dynamic Diesel Engine Operating Conditions. *Appl. Sci.* **2020**, *10*, 80. [\[CrossRef\]](#)
10. Ochoa, G.V.; Peñaloza, C.A.; Forero, J.D. Combustion and Performance Study of Low-Displacement Compression Ignition Engines Operating with Diesel–Biodiesel Blends. *Appl. Sci.* **2020**, *10*, 907. [\[CrossRef\]](#)
11. Krivtsova, N.I.; Gaga, S.G.; Desiatnichenco, A.A.; Popok, E.V.; Zaitceva, E.V. Synthetic Liquid Fuels Obtained by Thermolysis of Animal Waste. *Procedia Chem.* **2014**, *10*, 441–447. [\[CrossRef\]](#)
12. Gao, R.; Zhang, C.; Jun, K.W.; Seok, K.; Park, H.G.; Zhao, T.; Wang, L.; Wan, H.; Guan, G. Green liquid fuel and synthetic natural gas production via CO₂ hydrogenation combined with reverse water-gas-shift and Co-based Fischer-Tropsch synthesis. *J. CO₂ Util.* **2021**, *51*, 101619. [\[CrossRef\]](#)
13. Zhang, Q.; Fu, X. A Neural Network Fuzzy Energy Management Strategy for Hybrid Electric Vehicles Based on Driving Cycle Recognition. *Appl. Sci.* **2020**, *10*, 696. [\[CrossRef\]](#)
14. Morales-Morales, J.; Rivera-Cruz, M.A.; Cruz-Alcantar, P.; Bautista Santos, H.; Cervantes-Camacho, I.; Reyes Herrera, V.A. Performance Analysis of a Hybrid Electric Vehicle with Multiple Converter Configuration. *Appl. Sci.* **2020**, *10*, 1074. [\[CrossRef\]](#)
15. Anselma, P.G. Computationally efficient evaluation of fuel and electrical energy economy of plug-in hybrid electric vehicles with smooth driving constraints. *Appl. Energy* **2022**, *307*, 118247. [\[CrossRef\]](#)
16. Kim, D.M.; Lee, S.G.; Lim, M.S. Sizing and optimization process of hybrid electric propulsion system for heavy-duty vehicle based on Gaussian process modeling considering traction motor characteristics. *Renew. Sustain. Energy Rev.* **2022**, *161*, 112286. [\[CrossRef\]](#)
17. de Carlo, V.; Scalabrini, S.; Bisci, P.; Cocozza, P.; Formica, V.; Irlando, F.; Numidi, F.; Pedrazzani, G.G.; Spoto, M.M.; Vassallo, A. The New General Motors 2.0L Diesel 4-Cylinder Engine. In Proceedings of the 42nd International Vienna Motor Symposium, Vienna, Austria, 29–30 April 2021; published in an anthology. ISBN 978-3-9504969-0-1.
18. Helbing, C.C.; Köhne, M.; Kassel, T.; Herbst, T.T.; Wietholt, B.; Schleyer, J.J.; Kraus, S.; Düsterhöft, M.; Groenendijk, A.; Büchner, S.; et al. Making Transport Tasks Clean and Efficient—The New TDI Engines in the Volkswagen Commercial Vehicles. In Proceedings of the 42nd International Vienna Motor Symposium, published in an anthology. Vienna, Austria, 29–30 April 2021; ISBN 978-3-9504969-0-1.
19. Beatrice, C.; Di Blasio, G.; Belgiorno, G.; Avolio, G.; Pesce, F.C.; Vassallo, A. Balancing Hydraulic Flow and Fuel Injection Parameters for Low Emission and High-Efficiency Automotive Diesel Engines. *SAE Int. J. Adv. Curr. Pract. Mobil.* **2019**, *2*, 638–652. [\[CrossRef\]](#)
20. Han, S.W.; Shin, Y.S.; Kim, H.C.; Gee-Soo Lee, G.S. Study on the Common Rail Type Injector Nozzle Design Based on the Nozzle Flow Model. *Appl. Sci.* **2020**, *10*, 549. [\[CrossRef\]](#)
21. Belgiorno, G.; Boscolo, A.; Dileo, G.; Pesce, F.; Vassallo, A.; Beatrice, C.; Di Blasio, G.; Iannello, R. Experimental Study of Additive-Manufacturing-Enabled Innovative Diesel Combustion Bowl Features for Achieving Ultra-low Emissions and High Efficiency. *SAE Int. J. Adv. Curr. Pract. Mobil.* **2020**, *3*, 672–684. [\[CrossRef\]](#)
22. Han, Z. *Simulation and Optimization of Internal Combustion Engines*; SAE International: Warrendale, PA, USA, 2022; pp. 310–311. ISBN1 978-1-4686-0400-9; ISBN2 978-1-4686-0401-6; ISBN3 978-1-4686-0402-3. [\[CrossRef\]](#)
23. Hofbauer, P. Internal Combustion Engine with a Single Crankshaft and Having Opposed Cylinders with Opposed Pistons. U.S. Patent n. US 6,170,443, B1; Santa Barbara, 9 January 2001.

Disclaimer/Publisher’s Note: The statements, opinions and data contained in all publications are solely those of the individual author(s) and contributor(s) and not of MDPI and/or the editor(s). MDPI and/or the editor(s) disclaim responsibility for any injury to people or property resulting from any ideas, methods, instructions or products referred to in the content.